JOURNAL OF THE ROYAL SOCIETY Interface

Contact inhibition of locomotion probabilities drive solitary versus collective cell migration

Ravi A. Desai, Smitha B. Gopal, Sophia Chen and Christopher S. Chen

J. R. Soc. Interface 2013 **10**, 20130717, published 18 September 2013

JOURNAL OF THE ROYAL SOCIETY Interface

rsif.royalsocietypublishing.org

Research

Cite this article: Desai RA, Gopal SB, Chen S, Chen CS. 2013 Contact inhibition of locomotion probabilities drive solitary versus collective cell migration. J R Soc Interface 10: 20130717. http://dx.doi.org/10.1098/rsif.2013.0717

Received: 5 August 2013
Accepted: 27 August 2013

Subject Areas:
bioengineering, biophysics, systems biology

Keywords:
contact inhibition of locomotion, cell migration, micropatterning, cell–cell adhesion, cell polarization

Author for correspondence:
Christopher S. Chen
e-mail: chencs@bu.edu

†Present address: Medical Research Council, National Institute for Medical Research, London, UK and University College London, London, UK.
‡Present address: Department of Biomedical Engineering, Boston University, Boston, MA, USA and Wyss Institute for Biologically Inspired Engineering, Harvard University, Boston, MA, USA.

Electronic supplementary material is available at http://dx.doi.org/10.1098/rsif.2013.0717 or via http://rsif.royalsocietypublishing.org.

Royal Society Publishing
Informing the science of the future

Contact inhibition of locomotion probabilities drive solitary versus collective cell migration

Ravi A. Desai[1,2,†], Smitha B. Gopal[1], Sophia Chen[1] and Christopher S. Chen[1,‡]

[1]Department of Bioengineering, University of Pennsylvania, Philadelphia, PA, USA
[2]Max Planck Institute for Molecular Cell Biology and Genetics, Dresden, Germany

Contact inhibition of locomotion (CIL) is the process whereby cells collide, cease migrating in the direction of the collision, and repolarize their migration machinery away from the collision. Quantitative analysis of CIL has remained elusive because cell-to-cell collisions are infrequent in traditional cell culture. Moreover, whereas CIL predicts mutual cell repulsion and 'scattering' of cells, the same cells *in vivo* are observed to undergo CIL at some developmental times and collective cell migration at others. It remains unclear whether CIL is simply absent during collective cell migration, or if the two processes coexist and are perhaps even related. Here, we used micropatterned stripes of extracellular matrix to restrict cell migration to linear paths such that cells polarized in one of two directions and collisions between cells occurred frequently and consistently, permitting quantitative and unbiased analysis of CIL. Observing repolarization events in different contexts, including head-to-head collision, head-to-tail collision, collision with an inert barrier, or no collision, and describing polarization as a two-state transition indicated that CIL occurs probabilistically, and most strongly upon head-to-head collisions. In addition to strong CIL, we also observed 'trains' of cells moving collectively with high persistence that appeared to emerge from single cells. To reconcile these seemingly conflicting observations of CIL and collective cell migration, we constructed an agent-based model to simulate our experiments. Our model quantitatively predicted the emergence of collective migration, and demonstrated the sensitivity of such emergence to the probability of CIL. Thus CIL and collective migration can coexist, and in fact a shift in CIL probabilities may underlie transitions between solitary cell migration and collective cell migration. Taken together, our data demonstrate the emergence of persistently polarized, collective cell movement arising from CIL between colliding cells.

1. Introduction

Contact inhibition of locomotion (CIL) refers to cessation of cell migration in the direction of cell–cell collision [1–3]. Cessation of movement is rapidly followed by repolarization of the migration machinery away from the collision [4–10]. CIL operates in many cell types [2,6,11–15], is critical for coordination of cell movements in multicellular settings and has recently been implicated during migration in developing *Xenopus laevis*, *Danio rerio* and *Drosophila melanogaster* [5,7,16–18] as well as during invasive prostate cancer progression [6].

Despite recognition of CIL over half a century ago, methods for its *in vitro* study have remained largely unchanged, and involve either placing two tissue explants in close proximity in culture, or directly observing rare, serendipitous collisions between dissociated cells [1,3,4,19,20]. As a result, these methods have limited quantitative insight into CIL. The strength and lifetime of the CIL signal as well as the frequency and extent of the CIL response are not known, making it difficult to build quantitative models that explain collective cell behaviour. For example, CIL predicts that cells repolarize away from other cells upon collision, leading to a well-dispersed population of single

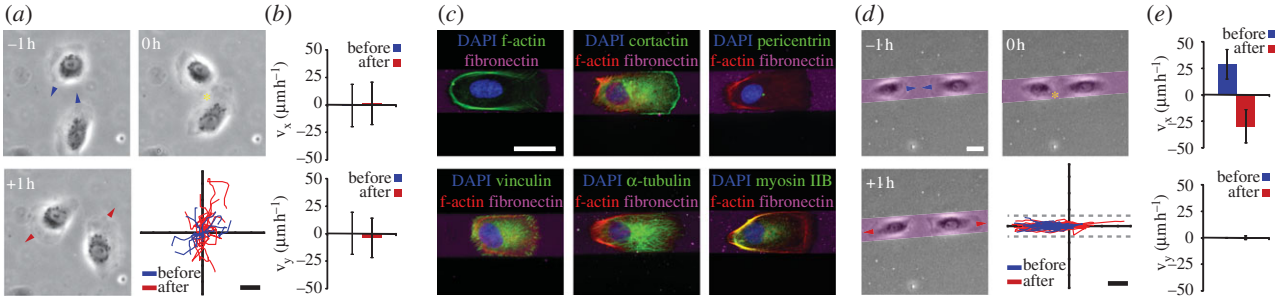

Figure 1. Patterned culture reveals cell repolarization. (*a*) Time-lapse microscopy of cells 6–20 h after plating, and trajectories of 10 representative cells (lower right) 30 min before (blue) and after (red) the collision. In phase contrast micrographs, blue arrowheads indicate cell migration direction 1 h before the collision, yellow asterisk indicates the site of the collision at 0 h, and red arrowheads indicate the direction of cell migration 1 h after the collision. (*b*) *X*- and *y*-velocities of cells 30 min before (blue) and after (red) the collision. Means ± s.e. from three independent experiments. (*c*) Cells were fixed and immunostained 20 h after plating on micropatterns. (*d*,*e*) Time-lapse sequence, trajectories and velocities were measured as in (*a*,*b*) from cells on micropatterns. In (*d*), micropatterned stripes are indicated by purple shading. All scale bars, 25 μm.

cells. Yet, cells are often observed migrating *en masse* during development, disease and homeostasis [21,22]. Moreover, cells transition from isolated cells to multicellular aggregates and vice versa during different phases of morphogenesis [17,23–26]. Whether CIL is simply absent during such collective migrations, or the two processes coexist and are related remains unclear.

To address these limitations, we designed an experimental platform based on micropatterning with which to study CIL in detail. After confirming the existence of CIL in our cells, we found that CIL is probabilistic, is triggered most robustly by 'head-to-head' cell–cell contact and occurs statistically independently. An agent-based model based on these experimental data predicted the emergence of long 'trains' of cells from CIL between individual cells and was quantitatively verified experimentally. The appearance of trains was a function of the probability of CIL. Together, our data indicate the emergence of persistent, collective cell movement arising from CIL between colliding cells.

2. Material and methods

2.1. Cell culture and reagents

NRK-52E cells (ATCC) were chosen as model cells for migration, because they have broad leading edges and clearly demarcated polarity [10], and were cultured in 10% fetal bovine serum (Gibco, Carlsbad, CA) in Dulbecco's modified Eagle medium (Gibco). Cells were G_o-synchronized prior to plating on experimental substrates as in [27]. Reagents included: 4′,6-diamidino-2-phenylindole dihydrochloride (Sigma, Saint Louis, MO), phalloidin-AlexFluor-488 (Invitrogen), anti-pericentrin (Covance, Princeton, NJ), anti-α-tubulin (Sigma), anti-human fibronectin (Cappell, Burlingame, CA), and anti-myosin heavy chain IIB (Covance).

2.2. Micropatterned substrates

Surface and microwell patterns were generated via microcontact printing [28]. Physical barriers were formed by casting polydimethylsiloxane (PDMS; Dow Corning, Midland, MI) against a silicon wafer patterned with approximately 350 μm tall photoresist and cleaning with EtOH. For experiments in the electronic supplementary material, figure S2, the barrier was coated with 50 μg ml^{-1} protein A (Sigma) for 1 h at room temperature (RT), thoroughly rinsed, then coated with 10 μg ml^{-1} fc-E-cadherin (R&D, Minneapolis, MN) for 1 h at RT. The barrier was rinsed, dried and placed in conformal contact with the micropatterned substrate. The entire assembly was incubated in 0.2% (w/v) Pluronics F127 to prevent protein adsorption to exposed PDMS. For all PDMS barrier experiments, cells transiently expressed EGFP, and fibronectin conjugated to AlexaFluor-568 (Invitrogen) was used to visualize the micropattern.

2.3. Immunofluorescence and microscopy

Cells were fixed in pre-warmed 2% paraformaldehyde in microtubule stabilizing buffer (1 mM ethylene glycol tetraacetic acid, 1 mM $MgSO_4$, 4% (w/v) poly(ethylene glycol) 8000 and 1% (v/v) Triton X 100 in 0.1 M piperazine-1,4-bis(2-ethanesulfonic acid), pH 6.75) for 10 min at 37°C, and labelled with antibodies in 10% goat serum. Fixed samples were imaged via widefield epifluorescence with a 63×, NA 1.4 Plan Apochromat objective on a Zeiss AxioVert 200M, and images were acquired with an AxioCam HRm using AxioVision software (Carl Zeiss, Thornwood, NY). Live samples were imaged via phase contrast microscopy with a 10×, NA 0.3 Plan Fluor objective, and a custom-built environmental chamber mounted on a Nikon Eclipse Ti with the Nikon perfect focus system (Nikon Instruments, Melville, NY), using a Hamamatsu C4742 camera (Hamamatsu Corporation, Bridgewater, NJ) and MetaMorph software (Molecular Devices, Downingtown, PA).

2.4. Experimental measurement of repolarization

Repolarization was determined from phase contrast, time-lapse recordings using a 10×, NA 0.3 Plan Fluor objective and a time interval of 4 min. Morphological repolarization was defined as a cell entering the collision with its lamellipodium facing the opposite cell before collision but after collision redirecting the lamellipodium away from the opposite cell, concurrent with migration away from the site of collision and opposite cell (figure 1*d* and electronic supplementary material, movie S2). The proportion of total cells observed that repolarized within a specific time interval (Δt) was recorded and plotted as a cumulative probability in figure 2*c*. Polarization was described as a two-state transition (equation (3.1)), and the repolarization rate was calculated as per equation (3.3) with the appropriate value of Δt.

2.5. Agent-based model

We created an agent-based model to predict the result of head-to-head collisions between two single cells or between a single cell and a train of cells. The model was formulated according to the following rules.

— An agent was defined as either a single cell or a train of cells, and had a speed and polarization as prescribed below.

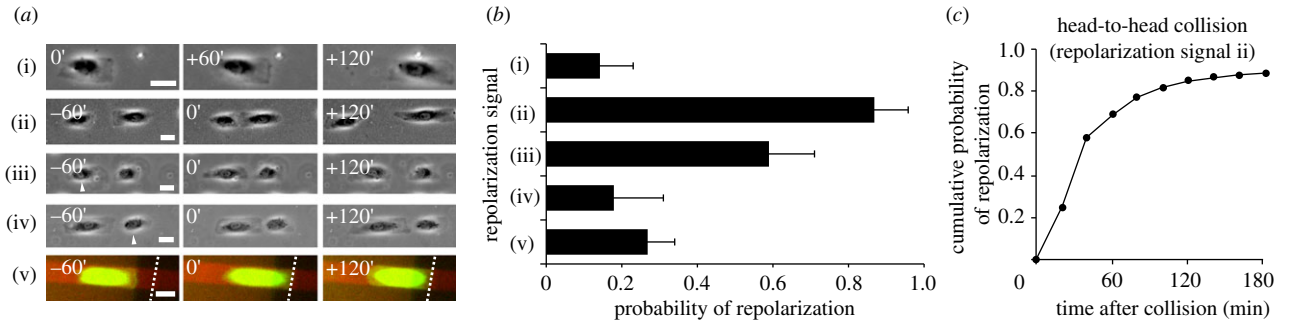

Figure 2. CIL is triggered upon head-to-head collision between cells. (*a*) Time-lapse microscopy of cells 6–20 h after plating, showing (i) persistent migration of a single cell, (ii) head-to-head collision between cells, (iii) head-to-tail collision between cells in which the rear cell repolarizes and the (iv) lead cell remains persistent, and (v) collision of a cell with an inert barrier. In (v), transmitted light optics were poor, so the cell is expressing GFP (green), is migrating along a fluorescent, micropatterned stripe (red), and collides with an inert topographical barrier (dashed line). In (ii–v), the collision occurs at 0 min. All scale bars, 25 µm. (*b*) The probability of repolarizing within 2 h of (i) beginning a persistent migration, or (ii–v) colliding with another cell or barrier as indicated in (*a*). Arrowheads in (*a*) indicate the cell (rear or lead) whose probability was measured for (*b*). In (ii), either cell of the head-to-head collision was measured. (*c*) For head-to-head collisions between single cells (situation ii), 58% of total cells had repolarized within 40 min of the collision.

— The speed of each agent was 30 µm h^{-1}, unless the agent was within the collision distance (10 µm) of, and polarized toward, another agent. In the latter case, the speed was defined to be 0.
— The polarization of each agent was either left or right.
— Initial polarization was defined such that a head-to-head collision occurred early in model simulations.
— Polarization could change only when agents collided head-to-head (came within the collision distance). Such a head-to-head collision triggered a repolarization signal, characterized by a magnitude and lifetime. The magnitude was probabilistic (events min^{-1}), as based on experimental data (curve fit in figure 4*c*). The lifetime was varied systematically in the model (figure 6).

The timestep of model simulations was 1 min. In each timestep, the following steps were performed: (i) check for a collision, (ii) simulate repolarization if appropriate, (iii) simulate movement if appropriate, and (iv) update positions. These steps were iterated as long as specified (figure 6). At the end of the simulation, entrainment was measured by assessing whether the agents were polarized in the same direction and were within 15 µm of one another. Simulations were implemented in MATLAB (The MathWorks, Natick, MA), and at least 1000 simulations were performed per condition.

3. Results

We followed migration of dissociated NRK-52E cells on a two-dimensional surface via time-lapse microscopy and observed collisions between cells. It appeared that cells ceased migrating in direction of the collision, and repolarized such that they migrated in a different direction before the collision (figure 1*a* and electronic supplementary material, movie S1). However, fewer than 16% of cells collided with another single cell within a 12 h observation period, even after pre-selecting for cells that appeared on the verge of collision (data not shown). Moreover, average cell velocity both before and after the collisions was zero, because migration in this two-dimensional, unpatterned setting was unconstrained (figure 1*b*). Taken together, our observations suggested the existence of CIL in these cells, but also illustrated the difficulties of describing the process.

To direct cells to experience a high frequency of visually clear, head-to-head collisions, we micropatterned parallel stripes of fibronectin with a period of 25 µm. This width was chosen to be similar to cell size, and permitted us to constrain cell migration to quasi-one-dimensional tracks [29,30]. Cells localized polarity markers in a typical fashion on the micropatterns: cortactin localized to the leading edge, the centrosome preceded the nucleus in the direction of migration, α-tubulin accumulated near the front of migrating cells and myosin IIB accumulated in the rear (figure 1*c*). Cells migrated with a similar speed as on unpatterned surfaces (29 ± 14 µm h^{-1}), and spontaneously switched direction infrequently (figure 2*a*(i),*b*(i)). Time-lapse microscopy showed that 53% of cells underwent collisions with another single cell during a 12 h observation period (data not shown). Upon collision, cells remained in contact with the other cell for approximately 60 ± 5 min, indicative of transient 'co-attraction' between cells [31] (see electronic supplementary material, figure S1). Collision also frequently triggered repolarization. That is, cells entered the collision with their lamellipodium facing the opposite cell but repolarized their lamellipodium upon collision, and migrated away from the collision in opposite directions (figure 1*d* and electronic supplementary material, movie S2). In fact, the magnitude of velocity parallel to the micropatterns before and after the collision was similar, albeit oppositely polarized (figure 1*e*). We conclude that polarization and migration speed are similar on patterned versus unpatterned surfaces, but collisions on patterned surfaces occur more consistently and frequently compared with unpatterned surfaces.

The consistency of cell repolarizations on micropatterns permitted us to quantitatively analyse such events in different contexts. Individual cells that migrated on the stripes spontaneously repolarized with a probability of 0.14 ± 0.09 within 2 h of beginning a persistent migration (figure 2*a*(i),*b*(i) and electronic supplementary material, movie S3). By contrast, a cell that collided with another cell head-to-head repolarized with a probability of 0.87 ± 0.09 within 2 h of the collision (figure 2*a*(ii),*b*(ii) and electronic supplementary material, movie S2). We also observed occasional, 'rear-end' collisions between cells. In these situations, the lead cell repolarized with a probability of 0.18 ± 0.13 within 2 h of the collision, and the rear cell repolarized with a probability of 0.59 ± 0.12 within 2 h of the collision (figure 2*a*(iii)(iv),*b*(iii)(iv) and electronic supplementary material, movies S4 and S5).

Significantly lower repolarization of the lead cell (0.18 ± 0.13) compared with the rear cell (0.59 ± 0.12) suggests the rear cell encounters CIL signals from the lead cell, but not vice versa. Modest repolarization of the rear cell (0.59 ± 0.12) compared with head-to-head collision (0.87 ± 0.09) suggests that the CIL signal operates most efficiently when two leading edges of cell abut. The cumulative time distribution of repolarization probability following head-to-head collision between single cells indicated that 58% of cells (126 total cells over three experiments) had repolarized within 40 min of the collision (figure 2*c*). We conclude that CIL occurs probabilistically, operates most efficiently when two cells collide head-to-head, and largely occurs within 40 min of a head-to-head collision between single cells.

Physical presence of the opposing cell might trigger CIL by preventing forward motion and new cell–extracellular matrix adhesion. Indeed, topographical features can direct cell migration along ridges via contact guidance [32–34]. To address such topographically induced repolarization, previous studies examined collisions between live and fixed cells [2,14]. Because these studies found conflicting results as to whether topography was sufficient to induce repolarization, we tested whether topographically induced repolarization operates here. We placed a non-adhesive PDMS block perpendicular to the micropatterned stripes prior to seeding cells. Cells colliding with the barrier migrated in the opposite direction with a probability of 0.27 ± 0.07 (figure 2*a*(v),*b*(v) and electronic supplementary material, movie S6). This was higher than expected for spontaneous repolarization in the absence of such a barrier (0.14 ± 0.09), but lower than the probability observed following cell–cell collisions (0.87 ± 0.09). Coating the PDMS barrier with E-cadherin, the primary receptor involved in initial cell–cell adhesion, also did not induce repolarization: cells collided with the barrier, spread against it, and subsequently migrated on the barrier itself (see electronic supplementary material, figure S2 and movie S7). Thus, these results indicate that a physical barrier to forward migration is not sufficient to induce CIL. These data support our assertion that collision between single, living cells induces strong CIL.

The observed repolarization probabilities illustrate the relative strength of the CIL signal, but did not describe the repolarization probabilities in absolute terms. Because our experimental setting essentially restricted cell migration to a single plane, we described CIL with a two-state transition:

$$L \overset{k}{\Leftrightarrow} R. \tag{3.1}$$

In this description, the probability P of repolarizing in time interval Δt from left (L) to right (R) or vice versa was calculated as

$$P = 1 - \exp[-k \times \Delta t], \tag{3.2}$$

where k represents the repolarization rate in min^{-1}. Repolarization rates were obtained from the experimentally observed probabilities, by solving equation (3.2) for k:

$$k = \frac{-\ln(1-P)}{\Delta t}. \tag{3.3}$$

The repolarization rate can be interpreted as repolarization events per minute. Because the probabilities in figure 2*b* were computed over a 120 min interval, $\Delta t = 120$ min was used to compute k from these probabilities (see electronic supplementary material, figure S3). These data more clearly describe the extent to which head-to-head collisions trigger the strongest CIL signal. We conclude that cells on micropatterned lines repolarize with probabilities that can be described via a two-state transition.

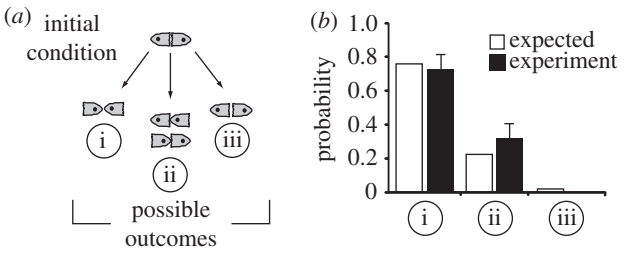

Figure 3. CIL operates statistically independently. (*a*) Upon a head-to-head collision between cells, (i) both, (ii) one or (iii) no cells can repolarize. (*b*) Expected (white bars) and experimentally observed (black bars) probabilities of the outcomes diagrammed in (*a*). The expected probability was computed using an CIL probability of 0.87 for each cell, and assumed cells repolarized statistically independently. Experimental measures in (*b*) represent the mean $\pm$ s.e. from three independent experiments.

Prior studies have not assessed whether CIL is a coupled response between two cells. To address this, we considered head-on collisions between single cells and asked whether CIL occurs statistically independently (figure 3*a*). Specifically, if CIL did not involve coupling between cells, we should expect to observe both, one and no cells repolarizing with probabilities of $(0.87) \times (0.87) = 0.76$, $(0.87) \times (1-0.87) \times 2 = 0.23$ and $(1-0.87) \times (1-0.87) = 0.02$, respectively (figure 3*b*, white bars). Our experimental results followed these expectations very closely (figure 3*b*, black bars), leading us to conclude that CIL occurs statistically independently, consistent with no coupling between cells.

Because repolarization rates were very high for cells engaging in head-to-head collisions, we expected that cells would remain well distributed as might occur with particles exhibiting mutually repulsive forces. Instead, we observed multicellular trains of closely contacting cells that migrated in a highly coherent and persistent manner (figure 4*a* and electronic supplementary material, movie S8). Moreover, immunofluorescent staining suggested that cells within such trains were stably coupled based on accumulation of E-cadherin at cell–cell contacts, and was supported by localization of actin and microtubule cytoskeletons between adjacent cells (figure 4*b*). These data are consistent with many studies showing that cells accumulate cadherins at contacts and juxtapose cytoskeletons upon cell–cell adhesion [35–37].

Interestingly, initial observations suggested that the persistence of trains appeared to be higher with longer trains. That is, upon collision with a single cell, longer trains were less likely to repolarize than shorter trains. To quantify this, we experimentally measured the probability of an n-cell train repolarizing within 40 min of a head-to-head collision with another cell, and observed a rapid decrease in repolarization with n (figure 4*c*). A curve fit of the relationship between the probability of repolarization, P, and number of cells, n, is given by $P(n) = \exp(-[(n-1)-\beta])$. The fit parameter β is found by the constraint that $P(n=1) = 0.58$ (figure 2*c*); here, $\beta = 0.546$. Although the curve fit is empirical, it captures the experimentally observed features that (i) $P(n=1) = 0.58$, (ii) P decreases rapidly with increasing n, and (iii) $P(n \to \infty) = 0$. Irrespective of mechanisms that cells engage when they are part of a train, we observe trains to move collectively and repolarize length-dependently.

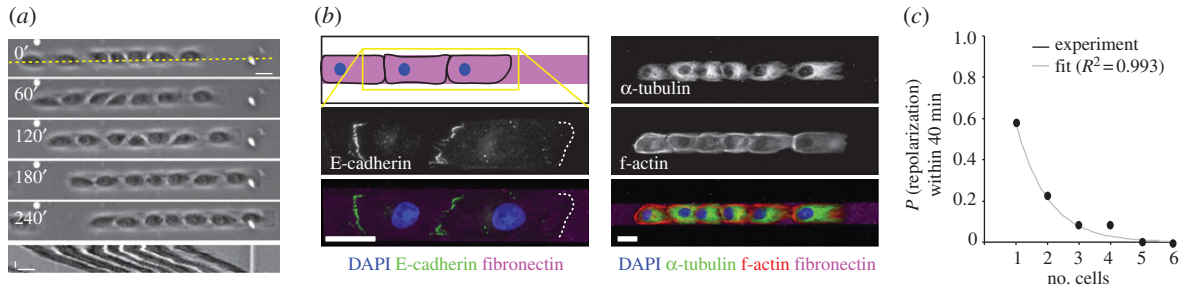

Figure 4. Trains behave as a coherent unit, and repolarize in a length-dependent manner. (*a*) Time-lapse microscopy of cells approximately 12–16 h after plating, showing a collective, persistent 'train' of seven cells. Panels with numbers are stills taken from a time-lapse sequence (see electronic supplementary material, movie S8). Bottom panel is a kymograph of time versus space, taken from the time-lapse sequence along the dashed yellow line drawn in the top panel. Numbers, time in minutes. Horizontal scale bars, 25 μm. Vertical scale bar, 1 h. (*b*) Immunofluorescent micrographs showing localization of E-cadherin (left) and microtubules and actin (right) in trains of cells on stripes of fibronectin. (*c*) Probability of repolarization of a train within 40 min of a head-to-head collision with a single cell versus number of cells in the train. Probabilities from at least three independent experiments (circles), and a curve fit of the data (grey). The curve fit equation is $P(n) = \exp(-[(n-1)-\beta])$, where P is probability, n is number of cells, and the fit parameter $\beta = 0.546$. See text for details.

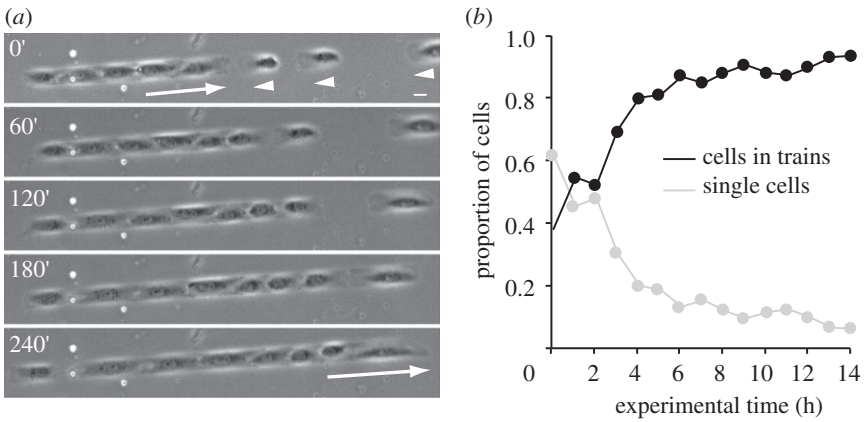

Figure 5. Collective, persistent trains of cells emerge from CIL between cells. (*a*) Time-lapse microscopy of cells approximately 12–16 h after plating, showing an example of multiple, single cells becoming entrained. Arrows indicate direction of train migration, and arrowheads indicate direction of migration of single cells at $t = 0$ min. Note that the train remains persistent throughout the sequence, whereas the single cells repolarize. Scale bar, 25 μm. (*b*) The proportion of single cells (grey) decreases with time and the proportion of cells in trains (black) increases with time. By 9 h, 88% of cells are in trains, and by 14 h, 93% of cells are in trains.

Such collectively moving trains could have arisen from pre-existing cell clusters that already were present during initial seeding onto the substrate, or could have emerged from collisions between single cells. Surprisingly, experimental observations suggested the latter: single cells became 'entrained' over the course of the experiment (figure 5*a* and electronic supplementary material, movie S9). Although the percentage of cells in trains at the beginning of the experiment was less than 40% of total cells, within 9 h this percentage had more than doubled to 88%, and by 14 h this percentage had eclipsed 93% (figure 5*b*). Together, our prior data indicated that CIL is operational in these cells, but we also observed the emergence of collectively migrating trains.

To reconcile these seemingly paradoxical observations, we constructed an agent-based model in which a cell collided head-to-head, on a stripe, with either another single cell or a train composed of two to six cells (figure 6*a*). In the model, collision triggered probabilistic repolarization as per the experimental probabilities we previously found (figure 4*c*). We converted probabilities to rates using equation (3.3) and $\Delta t = 40$ min. We systematically varied the length of time, τ, between the collision and duration over which the repolarization rate was non-zero. By iterating the model 1000 times, we measured the rate of entrainment (figure 6*b*). Our simulations predicted that, for $\tau = 80$ min, entrainment rapidly and monotonically increased with increasing train length (figure 6*c*, grey curve). That is, for increasing n, an n-cell train was increasingly likely to transition to an $n+1$ cell train upon head-to-head collision with a single cell.

To experimentally test this prediction, we measured the rate of entrainment following a head-to-head collision between a single cell and either another single cell or trains composed of two to six cells. We found good agreement between the model prediction and experimental data (figure 6*c*). To quantify the agreement, we computed R^2, which represents the extent to which the model captures experimental data. We computed R^2 while systematically varying τ to assess the optimal value of this free parameter in our model. We found that R^2 varied biphasically with τ, with an optimum R^2 at $\tau = 80$ min (figure 6*d*). We posit that for low τ, neither agent repolarizes, whereas for high τ, both agents repolarize. Only for intermediate values of τ does exactly one agent repolarize such that entrainment occurs. Our data indicate that the time between the signal trigger (collision) and cell response (entrainment) was 80 min.

In a head-to-head collision between single cells, a two-cell train will result only when exactly one of the cells repolarizes. We therefore reasoned that the probability of single cell polarization would affect the probability of a two-cell train emerging. Indeed, two-cell train emergence was quite sensitive

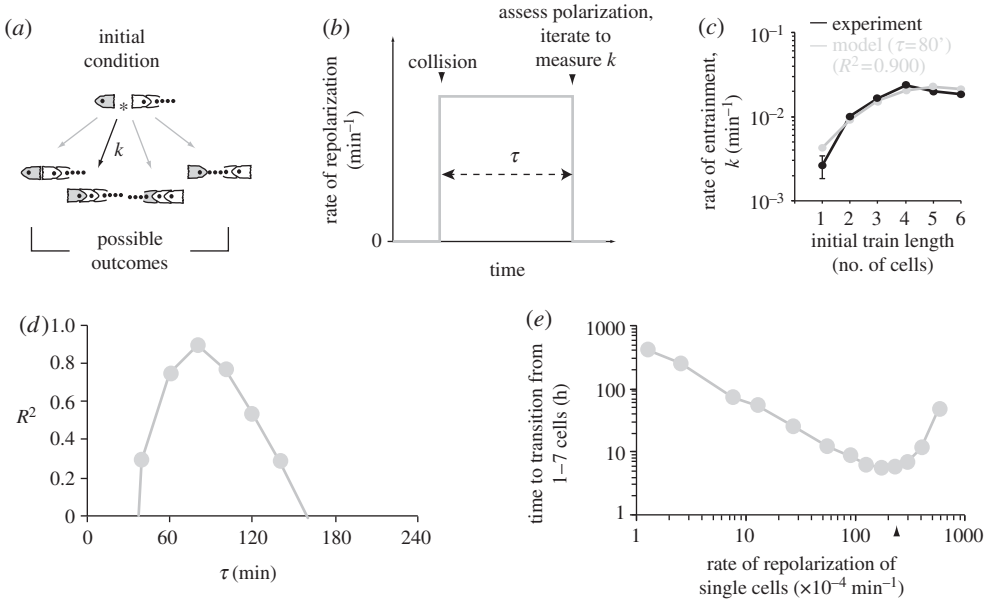

Figure 6. An agent-based model predicts the emergence of trains. (*a*) A head-to-head collision between a single cell and a train of cells can result in four outcomes. Entrainment, in which the single cell repolarizes but the train remains persistent, is indicated by the black arrow. The rate of this transition from a head-to-head collision to entrainment is indicated by *k*. (*b*) Schematic of the model, in which a collision triggers a non-zero rate of repolarization. The magnitude of the rate of repolarization is given by length-dependent repolarization as measured in figure 4*c*. The duration of the rate of polarization (τ) is systematically varied in model simulations. At the end of the simulation, the rate of entrainment *k* is measured. (*c*) Entrainment rate *k* versus train length, as predicted by the model for $\tau =$ 80 min (grey line) and measured experimentally (black line). Simulated rates are based on 1000 simulations. Experimental rates are based on at least three independent experiments. (*d*) R^2, a measure of experimental data predicted by the model, versus τ was computed to assess the ideal value of τ. Note that R^2 is maximum at $\tau = 80$ min. (*e*) The time for one cell to, through a series of head-to-head collisions and entrainments, give rise to a seven-cell train was computed based on model predictions versus single cell repolarization rate. Arrowhead, experimentally observed rate (2.2×10^{-2} min^{-1}).

to the single cell repolarization probability, as predicted by our model (see electronic supplementary material, figure S5a). Furthermore, the rate of entrainment (an *n*-cell train colliding head-to-head with a single cell, giving rise to an $n+1$ cell train) depended on the single cell repolarization rate, as predicted by our model (see electronic supplementary material, figure S5b). Because the inverse of entrainment rate is the time it takes for entrainment to occur, we calculated the expected time for a single cell to give rise to a seven-cell train, through iterative head-to-head collisions and entrainments. There was a clear minimum time at which trains emerged that depended on the rate at which single cells repolarized (figure 6*e*). Our experimentally observed single cell repolarization rate was remarkably close to this minimum (figure 6*e*). Although we intentionally remain agnostic of the molecular mechanism underlying changes in CIL probability, we conclude that CIL and collective migration not only coexist, but may be functionally related.

4. Discussion

Traditional culture suggested the presence of CIL, but was fraught with challenges including rare collisions, uncertainty surrounding how to categorize collisions, and lack of precision in defining repolarization. Micropatterns and modelling addressed these challenges permitting a large number of frequent, reproducible and quantifiable cell–cell collisions, and generating precise, quantitative and experimentally falsifiable predictions, respectively. Experiments on micropatterns revealed that CIL is a probabilistic event, head-to-head collision between cells induced the most robust CIL, cells repolarized statistically independently and the probability of a train repolarizing depended on the number of cells within the train. Based on these data, we formulated a model that predicted monotonically increasing entrainment with length of the train; this novel prediction was quantitatively verified experimentally. Together, these findings highlight the utility of our dual approach combining micropatterning and modelling.

The CIL signal upon head-to-head collision between individual cells was strong relative to other repolarization signals. It has been shown in a variety of contexts that cell–cell contact triggers cell polarity [5,7,10,38,39]. In many cases, homophilic binding between cadherin receptors on adjacent cells underlies the polarity signal, although the specific cadherin isoform and downstream signalling pathways involved are perhaps context-specific. Moreover, binding of ephrin ligands to cognate Eph receptors has been shown to underlie CIL in several cell types, including neural crest cells and prostate cancer cells [6,15,40]. Despite these inroads in understanding that highlight which molecules might be involved in the process, no study to date has quantitatively described the probabilistic nature of CIL, its relative strength, and its dependence on context. Our data revealed the stochasticity of CIL triggered by cell–cell collision and suggest that the context of cell–cell collisions (e.g. head-to-head versus head-to-tail) could have important effects on this CIL signal.

Why spontaneous repolarization in freely migrating cells is infrequent remains unclear. Cell–matrix adhesions are well known to direct cytoskeletal structure [41–45] and can trigger polarity signals via activation of Cdc42 and actin polymerization [46–48]. In contrast to the repulsive effects of cell–cell adhesions, cell–matrix adhesions appear to attract cell polarity via a process that could be called 'adhesion promotion of locomotion' (APL). It may be that CIL and APL alone can explain some of the differences in repolarization rates observed between pairs of cells. For example, upon

head-to-head collisions cells lose an APL signal and gain a CIL signal; we observed that both cells are likely to repolarize. Similarly, upon head-to-tail collisions the lead cell receives APL and CIL signals that act synergistically in the migratory direction, whereas the tail cell receives an APL signal in the migratory direction but a CIL signal in the direction opposite migration. Consistently, we observed that the lead cell most likely persists and the rear cell most likely repolarizes. We propose that freely migrating cells receive APL signals from cell–matrix adhesions to confer persistence but no CIL signals to induce repolarization, and therefore are predominantly persistent.

We observed trains of cells form over time, and posit that once formed these trains are an integrated, coherent unit rather than a collection of independently acting cells. First, the actin cytoskeleton of a train of cells resembled that of a single cell (compare figure 1*c* with figure 4*b*): f-actin accumulated at the sides and rear of both single cells and entire trains of cells. Second, trains repolarize collectively and length-dependently (figure 4*c*), indicating that trains migrate as a collective. Third, entire trains spread and migrate on an E-cadherin-coated barrier with similar probability as single cells (see electronic supplementary material, figure S2b). Because trains accumulate E-cadherin at cell–cell adhesions as expected (figure 4*b*), we hypothesize that cell–cell adhesions within trains signal differently from newly formed cell–cell adhesions that induce CIL. Indeed, cell–cell adhesions reinforce in response to exogenous force [49–51], and cell–cell adhesion triggers rearrangement of the cytoskeleton [10,35,52]. It is possible that an interplay between cell–matrix and cell–cell adhesions underlies the difference in how cell–cell adhesions signal in trains versus initial E-cadherin-mediated binding: vinculin, well-studied for its role in regulating cell–matrix adhesion, has been implicated in regulating mechanosensing at cadherin-based cell–cell junctions [53,54]. Moreover, in contexts ranging from convergent extension during embryonic morphogenesis to cancer metastasis, cell–matrix and cell–cell adhesion systems are intimately connected [55]. In light of this evidence, it would be surprising if cell–matrix and cell–cell adhesion systems did *not* interact to mediate CIL.

Our relatively simple experimental setting does have the limitation that migration is restricted to essentially one dimension, but it may nonetheless be relevant to a number of physiologic migration patterns. Specifically, migration patterns normally ascribed to two or three dimensions such as fibrillar migration, capillary sprouting or lateral-line migration in the zebrafish embryo may be mimicked by the standardized 'one-dimensional' setting studied here [30,56–58]. We predict a biphasic relationship between the probability of CIL and the emergence of collective cell migration (figure 6*e*): when CIL is either unlikely or very likely collective cell migration emerges very slowly, only intermediate CIL probabilities rapidly give rise to collective cell migration. Thus, by tuning the CIL probability cells might transition from solitary to collective migration and vice versa with more or less rapidity. Rapid transitions between solitary and collective migration have been observed for example during embryonic development when macrophages migrate collectively along the ventral axis then solitarily in a classic CIL manner [16,17], or upon starvation in *Dictyostelium discoideum* when cells transition from solitary to collective migration [59]. Our study reveals that CIL is a probabilistic process, and this stochasticity could drive transitions between solitary and collective cell migration. This experimental setting can be more closely linked to physiologic migration patterns by, for example, changing the width of the stripes, the cell type(s), the chemistry and mechanics of the substrate, and the growth media composition. It would be interesting, for example, to place cells from differing stages of embryogenesis or cancer progression in our assay to assess their ability to undergo CIL and collective migration.

The migration dynamics of cell populations are critical to multicellular organisms. Efforts to describe such dynamics in cells are largely focused on single phenomenon, and as such behaviours such as CIL, collective migration and single cell motility are largely thought of as unrelated processes. By contrast, our studies show that CIL, entrainment and collective migration are in fact linked. Interestingly, our model suggests that depending on the likelihood of CIL, population dynamics could shift between modes of migration, and this could perhaps underlie differences observed between cell types and contexts [21,22]. The strategy by which local interactions give rise to global migration patterns is not unlike that used by collectively behaving groups of animals [60,61], and perhaps represents a biological strategy whereby individuals act autonomously to influence collective behaviour [62–64]. Our data therefore highlight the abilities of cells to not only probe their local environment via local interactions, but also use such local interactions as a mechanism to give rise to collective behaviour.

Acknowledgements. We thank D. Jörg, K. Lee, J. Currie, G. Valentin and L. Morelli for reading the manuscript and providing critical feedback.
Funding statement. R.D. acknowledges financial support from the NSF Graduate Research Fellowship Programme and the Whitaker International Programme. This work was supported by NIH (HL073305) and the Penn Center for Engineering Cells and Regeneration.

References

1. Abercrombie M. 1979 Contact inhibition and malignancy. *Nature* **281**, 259–262. (doi:10.1038/281259a0)
2. Abercrombie M. 1970 Contact inhibition in tissue culture. *In Vitro* **6**, 128–142. (doi:10.1007/BF02616114)
3. Abercrombie M, Heaysman JE. 1953 Observations on the social behaviour of cells in tissue culture. I. Speed of movement of chick heart fibroblasts in relation to their mutual contacts. *Exp. Cell Res.* **5**, 111–131. (doi:10.1016/0014-4827(53)90098-6)
4. Paddock SW, Dunn GA. 1986 Analysing collisions between fibroblasts and fibrosarcoma cells: fibrosarcoma cells show an active invasionary response. *J. Cell Sci.* **81**, 163–187.
5. Carmona-Fontaine C, Matthews HK, Kuriyama S, Moreno M, Dunn GA, Parsons M, Stern CD, Mayor R. 2008 Contact inhibition of locomotion *in vivo* controls neural crest directional migration. *Nature* **456**, 957–961. (doi:10.1038/nature07441)
6. Astin JW, Batson J, Kadir S, Charlet J, Persad RA, Gillatt D, Oxley JD, Nobes CD. 2010 Competition amongst Eph receptors regulates contact inhibition of locomotion and invasiveness in prostate cancer cells. *Nat. Cell Biol.* **12**, 1194–1204. (doi:10.1038/ncb2122)
7. Theveneau E, Marchant L, Kuriyama S, Gull M, Moepps B, Parsons M, Mayor R. 2010 Collective chemotaxis requires contact-dependent cell

polarity. *Dev. Cell* **19**, 39–53. (doi:10.1016/j.devcel.2010.06.012)

8. Middleton CA. 1977 The effects of cell–cell contact on the spreading of pigmented retina epithelial cells in culture. *Exp. Cell Res.* **109**, 349–359. (doi:10.1016/0014-4827(77)90014-3)
9. Kadir S, Astin JW, Tahtamouni L, Martin P, Nobes CD. 2011 Microtubule remodelling is required for the front-rear polarity switch during contact inhibition of locomotion. *J. Cell Sci.* **124**, 2642–2653. (doi:10.1242/jcs.087965)
10. Desai RA, Gao L, Raghavan S, Liu WF, Chen CS. 2009 Cell polarity triggered by cell–cell adhesion via E-cadherin. *J. Cell Sci.* **122**, 905–911. (doi:10.1242/jcs.028183)
11. Middleton CA. 1972 Contact inhibition of locomotion in cultures of pigmented retina epithelium. *Exp. Cell Res.* **70**, 91–96. (doi:10.1016/0014-4827(72)90185-1)
12. Vaughan RB, Trinkaus JP. 1966 Movements of epithelial cell sheets *in vitro*. *J. Cell Sci.* **1**, 407–413.
13. Huttenlocher A, Lakonishok M, Kinder M, Wu S, Truong T, Knudsen KA, Horwitz AF. 1998 Integrin and cadherin synergy regulates contact inhibition of migration and motile activity. *J. Cell Biol.* **141**, 515–526. (doi:10.1083/jcb.141.2.515)
14. Vesely P, Weiss RA. 1973 Cell locomotion and contact inhibition of normal and neoplastic rat cells. *Int. J. Cancer* **11**, 64–76. (doi:10.1002/ijc.2910110108)
15. Tanaka M, Kuriyama S, Aiba N. 2012 Nm23-H1 regulates contact inhibition of locomotion, which is affected by ephrin-B1. *J. Cell Sci.* **125**, 4343–4353. (doi:10.1242/jcs.104083)
16. Stramer B *et al*. 2010 Clasp-mediated microtubule bundling regulates persistent motility and contact repulsion in *Drosophila* macrophages *in vivo*. *J. Cell Biol.* **189**, 681–689. (doi:10.1083/jcb.200912134)
17. Davis JR, Huang CY, Zanet J, Harrison S, Rosten E, Cox S, Soong DY, Dunn GA, Stramer BM. 2012 Emergence of embryonic pattern through contact inhibition of locomotion. *Development* **139**, 4555–4560. (doi:10.1242/dev.082248)
18. Theveneau E, Steventon B, Scarpa E, Garcia S, Trepat X, Streit A, Mayor R. 2013 Chase-and-run between adjacent cell populations promotes directional collective migration. *Nat. Cell Biol.* **15**, 763–772. (doi:10.1038/ncb2772)
19. Abercrombie M, Ambrose EJ. 1958 Interference microscope studies of cell contacts in tissue culture. *Exp. Cell Res.* **15**, 332–345. (doi:10.1016/0014-4827(58)90034-X)
20. Anear E, Parish RW. 2012 The effects of modifying RhoA and Rac1 activities on heterotypic contact inhibition of locomotion. *FEBS Lett.* **586**, 1330–1335. (doi:10.1016/j.febslet.2012.03.044)
21. Friedl P, Gilmour D. 2009 Collective cell migration in morphogenesis, regeneration and cancer. *Nat. Rev. Mol. Cell Biol.* **10**, 445–457. (doi:10.1038/nrm2720)
22. Rorth P. 2007 Collective guidance of collective cell migration. *Trends Cell Biol.* **17**, 575–579. (doi:10.1016/j.tcb.2007.09.007)
23. McCann CP, Kriebel PW, Parent CA, Losert W. 2010 Cell speed, persistence and information transmission during signal relay and collective migration. *J. Cell Sci.* **123**, 1724–1731. (doi:10.1242/jcs.060137)
24. Bronner-Fraser M, Fraser SE. 1988 Cell lineage analysis reveals multipotency of some avian neural crest cells. *Nature* **335**, 161–164. (doi:10.1038/335161a0)
25. Richardson BE, Lehmann R. 2010 Mechanisms guiding primordial germ cell migration: strategies from different organisms. *Nat. Rev. Mol. Cell Biol.* **11**, 37–49. (doi:10.1038/nrm2815)
26. Tarbashevich K, Raz E. 2010 The nuts and bolts of germ-cell migration. *Curr. Opin. Cell Biol.* **22**, 715–721. (doi:10.1016/j.ceb.2010.09.005)
27. Liu WF, Nelson CM, Pirone DM, Chen CS. 2006 E-cadherin engagement stimulates proliferation via Rac1. *J. Cell Biol.* **173**, 431–441. (doi:10.1083/jcb.200510087)
28. Tan JL, Liu W, Nelson CM, Raghavan S, Chen CS. 2004 Simple approach to micropattern cells on common culture substrates by tuning substrate wettability. *Tissue Eng.* **10**, 865–872. (doi:10.1089/1076327041348365)
29. Fraley SI, Feng Y, Giri A, Longmore GD, Wirtz D. 2012 Dimensional and temporal controls of three-dimensional cell migration by zyxin and binding partners. *Nat. Commun.* **3**, 719. (doi:10.1038/ncomms1711)
30. Pouthas F, Girard P, Lecaudey V, Ly TB, Gilmour D, Boulin C, Pepperkok R, Reynaud EG. 2008 In migrating cells, the Golgi complex and the position of the centrosome depend on geometrical constraints of the substratum. *J. Cell Sci.* **121**, 2406–2414. (doi:10.1242/jcs.026849)
31. Carmona-Fontaine C, Theveneau E, Tzekou A, Tada M, Woods M, Page KM, Parsons M, Lambris JD, Mayor R. 2011 Complement fragment C3a controls mutual cell attraction during collective cell migration. *Dev. Cell* **21**, 1026–1037. (doi:10.1016/j.devcel.2011.10.012)
32. Teixeira AI, Abrams GA, Bertics PJ, Murphy CJ, Nealey PF. 2003 Epithelial contact guidance on well-defined micro- and nanostructured substrates. *J. Cell Sci.* **116**, 1881–1892. (doi:10.1242/jcs.00383)
33. Curtis AS, Varde M. 1964 Control of cell behavior: topological factors. *J. Natl Cancer Inst.* **33**, 15–26.
34. Rosenberg MD. 1963 Cell guidance by alterations in monomolecular films. *Science* **139**, 411–412. (doi:10.1126/science.139.3553.411)
35. Kovacs EM, Goodwin M, Ali RG, Paterson AD, Yap AS. 2002 Cadherin-directed actin assembly: E-cadherin physically associates with the Arp2/3 complex to direct actin assembly in nascent adhesive contacts. *Curr. Biol.* **12**, 379–382. (doi:10.1016/S0960-9822(02)00661-9)
36. Smutny M *et al*. 2010 Myosin II isoforms identify distinct functional modules that support integrity of the epithelial zonula adherens. *Nat. Cell Biol.* **12**, 696–702. (doi:10.1038/ncb2072)
37. Cavey M, Rauzi M, Lenne PF, Lecuit T. 2008 A two-tiered mechanism for stabilization and immobilization of E-cadherin. *Nature* **453**, 751–756. (doi:10.1038/nature06953)
38. Dupin I, Camand E, Etienne-Manneville S. 2009 Classical cadherins control nucleus and centrosome position and cell polarity. *J. Cell Biol.* **185**, 779–786. (doi:10.1083/jcb.200812034)
39. Weber GF, Bjerke MA, DeSimone DW. 2012 A mechanoresponsive cadherin-keratin complex directs polarized protrusive behavior and collective cell migration. *Dev. Cell* **22**, 104–115. (doi:10.1016/j.devcel.2011.10.013)
40. Smith A, Robinson V, Patel K, Wilkinson DG. 1997 The EphA4 and EphB1 receptor tyrosine kinases and ephrin-B2 ligand regulate targeted migration of branchial neural crest cells. *Curr. Biol.* **7**, 561–570. (doi:10.1016/S0960-9822(06)00255-7)
41. Thery M, Pepin A, Dressaire E, Chen Y, Bornens M. 2006 Cell distribution of stress fibres in response to the geometry of the adhesive environment. *Cell Motil. Cytoskeleton* **63**, 341–355. (doi:10.1002/cm.20126)
42. Thery M, Racine V, Pepin A, Piel M, Chen Y, Sibarita JB, Bornens M. 2005 The extracellular matrix guides the orientation of the cell division axis. *Nat. Cell Biol.* **7**, 947–953. (doi:10.1038/ncb1307)
43. Thery M, Racine V, Piel M, Pepin A, Dimitrov A, Chen Y, Sibarita J-B, Bornens M. 2006 Anisotropy of cell adhesive microenvironment governs cell internal organization and orientation of polarity. *Proc. Natl Acad. Sci. USA* **103**, 19 771–19 776. (doi:10.1073/pnas.0609267103)
44. Chen CS, Alonso JL, Ostuni E, Whitesides GM, Ingber DE. 2003 Cell shape provides global control of focal adhesion assembly. *Biochem. Biophys. Res. Commun.* **307**, 355–361. (doi:10.1016/S0006-291X(03)01165-3)
45. Desai RA, Khan MK, Gopal SB, Chen CS. 2011 Subcellular spatial segregation of integrin subtypes by patterned multicomponent surfaces. *Integr. Biol.* (*Camb.*) **3**, 560–567. (doi:10.1039/c0ib00129e)
46. Etienne-Manneville S, Hall A. 2001 Integrin-mediated activation of Cdc42 controls cell polarity in migrating astrocytes through PKCzeta. *Cell* **106**, 489–498. (doi:10.1016/S0092-8674(01)00471-8)
47. Gomes ER, Jani S, Gundersen GG. 2005 Nuclear movement regulated by Cdc42, MRCK, myosin, and actin flow establishes MTOC polarization in migrating cells. *Cell* **121**, 451–463. (doi:10.1016/j.cell.2005.02.022)
48. Watanabe T *et al*. 2004 Interaction with IQGAP1 links APC to Rac1, Cdc42, and actin filaments during cell polarization and migration. *Dev. Cell* **7**, 871–883. (doi:10.1016/j.devcel.2004.10.017)
49. Chu YS, Thomas WA, Eder O, Pincet F, Perez E, Thiery JP, Dufour S. 2004 Force measurements in E-cadherin-mediated cell doublets reveal rapid adhesion strengthened by actin cytoskeleton remodeling through Rac and Cdc42. *J. Cell Biol.* **167**, 1183–1194. (doi:10.1083/jcb.200403043)
50. Yonemura S, Wada Y, Watanabe T, Nagafuchi A, Shibata M. 2010 α-Catenin as a tension transducer

that induces adherens junction development. *Nat. Cell Biol.* **12**, 533–542. (doi:10.1038/ncb2055)

51. Liu Z, Tan JL, Cohen DM, Yang MT, Sniadecki NJ, Ruiz SA, Nelson CM, Chen CS. 2010 Mechanical tugging force regulates the size of cell–cell junctions. *Proc. Natl Acad. Sci. USA* **107**, 9944–9949. (doi:10.1073/pnas.0914547107)
52. Ehrlich JS, Hansen MD, Nelson WJ. 2002 Spatio-temporal regulation of Rac1 localization and lamellipodia dynamics during epithelial cell–cell adhesion. *Dev. Cell* **3**, 259–270. (doi:10.1016/S1534-5807(02)00216-2)
53. le Duc Q, Shi Q, Blonk I, Sonnenberg A, Wang N, Leckband D, de Rooij J. 2010 Vinculin potentiates E-cadherin mechanosensing and is recruited to actin-anchored sites within adherens junctions in a myosin II-dependent manner. *J. Cell Biol.* **189**, 1107–1115. (doi:10.1083/jcb.201001149)
54. Leerberg JM, Yap AS. 2012 Vinculin, cadherin mechanotransduction and homeostasis of cell–cell junctions. *Protoplasma* **250**, 817–829. (doi:10.1007/s00709-012-0475-6)
55. Weber GF, Bjerke MA, Desimone DW. 2011 Integrins and cadherins join forces to form adhesive networks. *J. Cell Sci.* **124**, 1183–1193. (doi:10.1242/jcs.064618)
56. Dike LE, Chen CS, Mrksich M, Tien J, Whitesides GM, Ingber DE. 1999 Geometric control of switching between growth, apoptosis, and differentiation during angiogenesis using micropatterned substrates. *In Vitro Cell. Dev. Biol. Anim.* **35**, 441–448. (doi:10.1007/s11626-999-0050-4)
57. Doyle AD, Wang FW, Matsumoto K, Yamada KM. 2009 One-dimensional topography underlies three-dimensional fibrillar cell migration. *J. Cell Biol.* **184**, 481–490. (doi:10.1083/jcb.200810041)
58. Maiuri P *et al*. 2012 The first world cell race. *Curr. Biol.* **22**, R673–R675. (doi:10.1016/j.cub.2012.07.052)
59. Devreotes P. 1989 *Dictyostelium discoideum*: a model system for cell–cell interactions in development. *Science* **245**, 1054–1058. (doi:10.1126/science.2672337)
60. Couzin ID, Krause J. 2003 Self-organization and collective behavior in vertebrates. *Adv. Stud. Behav.* **32**, 1–75. (doi:10.1016/S0065-3454(03)01001-5)
61. Parrish JK, Edelstein-Keshet L. 1999 Complexity, pattern, and evolutionary trade-offs in animal aggregation. *Science* **284**, 99–101. (doi:10.1126/science.284.5411.99)
62. Vitorino P, Meyer T. 2008 Modular control of endothelial sheet migration. *Genes Dev.* **22**, 3268–3281. (doi:10.1101/gad.1725808)
63. Vedula SR, Leong MC, Lai TL, Hersen P, Kabla AJ, Lim CT, Ladoux B. 2012 Emerging modes of collective cell migration induced by geometrical constraints. *Proc. Natl Acad. Sci. USA* **109**, 12 974–12 979. (doi:10.1073/pnas.1119313109)
64. Trepat X, Wasserman MR, Angelini TE, Millet E, Weitz DA, Butler JP, Fredberg JJ. 2009 Physical forces during collective cell migration. *Nat. Phys.* **5**, 426–430. (doi:10.1038/nphys1269)